7-2021

Trends in Land Surface Phenology across the Conterminous United States (1982-2016) Analyzed by NEON Domains

Liang Liang
University of Kentucky, liang.liang@uky.edu

Geoffrey M. Henebry
Michigan State University, henebryg@msu.edu

Lingling Liu
Stanford University, lingling.liu@stanford.edu

Xiaoyang Zhang
South Dakota State University, xiaoyang.zhang@sdstate.edu

Li-Chih Hsu
Binghamton University, lhsu@binghamton.edu

Trends in Land Surface Phenology across the Conterminous United States (1982-2016) Analyzed by NEON Domains

Digital Object Identifier (DOI)
https://doi.org/10.1002/eap.2323

Notes/Citation Information
Published in *Ecological Applications*, v. 31, issue 5, e02323.

Trends in land surface phenology across the conterminous United States (1982-2016) analyzed by NEON domains

Liang Liang[1]*, Geoffrey M Henebry[2], Lingling Liu[3], Xiaoyang Zhang[4], Li-Chih Hsu[5]

[1]Department of Geography, University of Kentucky, Lexington, KY 40506, USA

[2]Department of Geography, Environment, and Spatial Sciences, and the Center for Global Change and Earth Observations, Michigan State University, East Lansing, MI 48824, USA

[3]Natural Capital Project, Woods Institute for the Environment, Stanford University, Stanford, CA 94305, USA

[4] Department of Geography and Geospatial Sciences, and the Geospatial Sciences Center of Excellence, South Dakota State University, Brookings, SD 57007, USA

[5]Department of Geography, Binghamton University, SUNY, Binghamton, NY 13902, USA

*Corresponding author, Email: liang.liang@uky.edu; Phone: +1 (859) 257-7058

Abstract

Tracking phenological change in a regionally explicit context is a key to understanding ecosystem status and change. The current study investigated long-term trends of satellite-observed land surface phenology (LSP) in the 17 National Ecological Observatory Network (NEON) domains across the conterminous United States (CONUS). Characterization of LSP trends was based on a high temporal resolution (3-day) time series of the two-band enhanced vegetation index (EVI2) derived from a long-term data record (LTDR) of the Advanced Very High Resolution Radiometer (AVHRR) and the Moderate Resolution Imaging Spectroradiometer (MODIS). We identified significant trend patterns in LSP and their seasonal climate and land use / land cover drivers for each NEON domain. Key findings include: (1) the start of season (SOS) predominantly shifted later in 13 out of 17 domains (24.3% of CONUS by area) due potentially to both a lack of spring warming in the eastern U.S. and changes in agronomic practices over agricultural lands; (2) the end of season (EOS) became predominantly later in 9 domains dominated by natural vegetation (14.1% of CONUS by area) in response to widespread warming in autumn; (3) the EOS predominantly shifted earlier in 3 domains (10.6% of CONUS by area) over primarily agricultural lands as potentially affected by changes in crop growth cycles; and (4) earlier shift in the SOS was mostly found in the Northwest (3.6% of CONUS by area) and was predominant only in the moist Pacific Northwest (27.7% of the domain by area) in response to more pronounced spring warming in the region. The overall patterns of SOS and EOS trends across CONUS appeared constrained by continental-scale temperature trends as characterized by a west-east dipole and the distribution of the nation's agricultural lands. In addition, seasonal trend analysis revealed that most NEON domains (15/17) became predominantly greener in part of or throughout the growing season, potentially contributed by

both climate change induced growth increase and improved agricultural productivity. The domain-wide LSP trends with their underlying drivers identified here provide important contextual information for NEON science as well as for investigations within CONUS using other distributed observatories (*e.g.*, LTER, LTAR, FLUXNET, USA-NPN, *etc.*).

Keywords

CONUS; seasonal trend analysis; vegetation phenology; climate change; land use / land cover; Warming Hole

Introduction

Remotely-sensed land surface phenology (LSP) tracks seasonal development in the vegetated land surface, which can be affected by climate variation, ecological disturbances, land use / land cover changes, and other natural processes and anthropogenic activities (de Beurs and Henebry 2004, Henebry and de Beurs 2013, Zhang 2018). Long-term observation of LSP typically relies on coarser spatial resolution (≥1 km) time series of vegetation indices (VI) derived from reflectance data acquired by satellite sensors such as the Advanced Very High Resolution Radiometer (AVHRR) onboard NOAA's Polar Orbiting Environmental Satellites since 1980s, and the Moderate Resolution Imaging Spectroradiometer (MODIS) onboard NASA's Terra and Aqua satellites since the early 2000s (Justice *et al.* 1986, Justice *et al.* 1998). These multi-decadal observational data have provided an opportunity to examine trends of phenological change over broad geographic regions. To identify such large-scale phenological trends clearly is important for tracking the status of vegetated land surface and ecosystems as influenced by changes both in climate and land use / land cover.

Phenological change expressed as the timing shift of important phenological events (e.g., breaking of leaf buds or coloration of fall foliage) has been recognized as a crucial indicator of climate change impacts on biospheric processes (Cleland *et al.* 2007, Morisette *et al.* 2009, Chmura *et al.* 2019, Weltzin *et al.* 2020). In contrast to the sharp phenological transitions observable in specific plants, the intrinsically mixed signals available from satellite observations require LSP to rely on phenometrics extracted from smooth annual trajectories of VIs, such as start of season (SOS), end of season (EOS), and growing season length (GSL) (Zhang *et al.* 2003, de Beurs and Henebry 2010). Studies using LSP since the 1980s have shown that a warming global climate has generally shifted SOS earlier and EOS later, thereby extending GSL in many regions across the extratropics (Julien and Sobrino 2009, Zhang *et al.* 2014, Piao *et al.* 2019). However, specific phenological shifts at a regional scale vary geographically with respect to direction (earlier *vs.* later), magnitude (shifts in days per decade), and the statistical significance of detected changes. Thus, it is fitting to examine regional patterns of both LSP trends and associated climatic drivers. In addition, it is appropriate to consider non-climatic factors such as changes in agricultural land use due to socioeconomic transitions (de Beurs and Henebry 2004) and agricultural practices (Nguyen *et al.* 2020), since anthropogenic activity can alter LSP across large areas (White *et al.* 2005b, Zhang *et al.* 2019).

Long-term trends of vegetation phenology over the conterminous United States (CONUS) have been investigated in previous studies, but with inconsistent findings. Reed (2006) studied LSP based on time series of AVHRR Normalized Difference Vegetation Index (NDVI, the difference between NIR and red reflectances divided by the sum of NIR and red reflectances; Tucker 1979) data over North America from 1982 through 2003, and found highly mixed trends for SOS (sporadic locations with either significant earlier or later trends), and more areas of significantly later EOS. Zhang *et al.* (2007) analyzed LSP from AVHRR NDVI data from 1982 to 2005 and highlighted a contrast between earlier SOS in the Northeast, Mid-Atlantic, and Upper Midwest and later SOS in the Southeast of the U.S., but also showed later SOS in the Midwestern Corn Belt. In a recent global-scale study using AVHRR NDVI time series for 1982-2012, Garonna *et al.* (2016) showed significantly later SOS and earlier EOS in a concentrated region in the Midwestern Corn Belt, and sporadic areas with significantly earlier SOS or later EOS across the study area, especially in southeastern Canada and bordering U.S. Northeast. Zhang *et al.* (2019) found later trends in SOS dates across croplands of the U.S. Midwest and Northern Great Plains at the state scale, attributing two-thirds of this phenological change between 1982-2014 to land use / land cover change. In particular, Yue *et al.* (2015) summarized previous phenological trend analyses over U.S. deciduous forests that used at least 20 years of data and clearly illustrated a disparity of results among the studies. Such inconsistency among different studies may arise for multiple reasons, such as different approaches to deriving phenometrics; different statistical methods used for trend extraction; varied lengths of study periods; and inherent data uncertainties. The disparity arising from differences of algorithms used for LSP detection and characterization was highlighted by White *et al.* (2009), who showed that up to two months of difference in SOS existed in estimates using different approaches with the same input data. In addition to cross-comparison of LSP timings with *in situ* observations (Liang *et al.* 2011), an alternative way to constrain such uncertainties is to establish more clearly the geographic relationships between observed LSP changes and their underlying drivers. This approach is based on the rationale that the direction and magnitude of LSP change in each area must be consistent with the nature and degree of changes attributable to climate and/or land use / land cover in that area. However, we acknowledge that observed phenological changes may arise from the interaction of multiple factors co-occurring at different scales in space and time.

Here we investigated LSP trends across CONUS with an emphasis on regional patterns of change in relation to specific drivers within the spatial framework of the National Ecological Observatory Network (NEON) domains (Schimel *et al.* 2007, Keller *et al.* 2008). Our fundamental research question was "What are the regional-scale geographic relationships between the spatial patterns of LSP trends and the spatial patterns of climatic and land use / land cover changes?". We aimed to increase understanding of the geographic coherency and consistency of the land surface phenological trends across the study area. We utilized a newer and improved long-term (1982-2016) time series of Enhanced Vegetation Index 2 data (EVI2; Zhang *et al.* 2014) derived from both AVHRR and MODIS with reference to the NEON domains to detect regional patterns of LSP trends. In addition to assessing interannual variations of the commonly used phenometrics that mark only the transition points (*viz.*, SOS, EOS, and GSL), we employed seasonal trend analysis (STA; Eastman *et al.* 2009) to evaluate changes to the shapes of annual EVI2 curves. STA complements the traditional phenometric-focused approach and provides additional characterization of the phenological change trends. We linked the detected phenological trend patterns with seasonal climatic variables and land use / land cover types for each of 17 NEON domains within CONUS. By focusing on significant changes within NEON domains, we evaluate and identify coherent geographic relationships between phenological trends and their underlying drivers and provide important contextual information to support the macrosystems inference intended for NEON (Keller *et al.* 2008, Collinge 2018, Knapp and Collins 2019).

Methods and Data

Land surface phenology data

The dataset used to derive land surface phenology (LSP) was based on daily land surface reflectances at a spatial resolution of 0.05° (~5 km at equator) from the AVHRR long-term data record (LTDR, AVH09C1 version 4) from 1982 to 1999 and MODIS Climate Modeling Grid (CMG, MOD09CMG, Collection 6) from 2000 to 2016 (Zhang 2015). The two-band Enhanced Vegetation Index (EVI2) derived from red and near-infrared reflectances was used due to its advantages over the commonly-used NDVI in terms of higher sensitivity to dense vegetation and lower sensitivities to soil background and non-green land surfaces during the winter (Huete *et al.* 2006, Jiang *et al.* 2008, Rocha and Shaver 2009, Zhang *et al.* 2018). The three-day EVI2 time series was constructed by selecting only good quality (based on QA ratings) data and smoothed using Savitzky-Golay filtering to attenuate irregular EVI2 variations. More details about EVI2 time series processing are available elsewhere (Zhang *et al.* 2014, Zhang 2015). A hybrid piecewise logistic model (HPLM; Zhang 2015) was applied to reconstruct the EVI2 temporal trajectories. The rate of curvature change in the HPLM fit was used to identify the phenological transition dates (phenometrics) marking the growing season, namely SOS and EOS. Finally, systematic differences between AVHRR-based and MODIS-based phenological time series were minimized using linear regression models (Liu *et al.* 2016). GSL was subsequently calculated as the difference between SOS and EOS. All LSP data were cropped to the extent of CONUS.

Climate and land use/land cover data

We used the gridded climate data for CONUS from the PRISM Climate Group, Oregon State University (http://prism.oregonstate.edu). Monthly temperature and precipitation values from 1982 to 2016 were downloaded and the 4 km grids were resampled to 0.05° using the nearest neighbor method to match the resolution of LSP data. Both monthly time series and seasonal weather variables were used in this study. For seasonal variable derivation, average temperatures and total precipitations for winter, spring, summer, and autumn seasons were computed for each year. Monthly data were grouped into respective seasons according to the following order: winter—November, December, January (NDJ); spring—February, March, April (FMA); summer—May, June, July (MJJ); and autumn—August, September, October (ASO). This method of dividing the year into seasons is one month offset from the typical meteorological seasons (*viz.*, spring—March, April, May (MAM), *etc.*) because plant phenology in the extratropics primarily responds to prior weather conditions (Liang 2019). For CONUS, weather in February is typically more influential on SOS timing than weather in May; likewise, weather in August is more important to EOS timing than weather in November. The winter and spring variables are more relevant to SOS, and the summer and autumn variables to EOS. For land cover information, we used the MODIS/Terra+Aqua Land Cover Type CMG 0.05° product (MCD12C1, Collection 6) for 2016 and associated the classes of the International Geosphere-Biosphere Programme (IGBP) land cover scheme with the detected LSP trends.

Trend analysis

We detected trends in SOS, EOS, and GSL time series from 1982-2016 using the non-parametric Theil-Sen median slope estimator (Hoaglin *et al.* 2000). For every pixel, slopes of all pairwise combinations of phenometric dates from all years were computed, and their median value was used to estimate a rate of change. The Theil-Sen median trend test has a breakdown bound and rejects interannual trends shorter than 29% of the time series length; therefore, it is insensitive to shorter interannual variation but reveals trends over a longer period. This robustness may help address the effect of an apparent slowing-down (hiatus) of global warming between 1998-2012 (Medhaug *et al.* 2017, Wang *et al.* 2019). We used the TerrSet Earth Trend Modeler developed by Clark Labs (Eastman *et al.* 2009) to perform the analyses and produced images of median trends along with their p-values (using the contextual Mann-Kendall test) over the study area for SOS, EOS, and GSL. We used the same approach to detect long-term trends in seasonal temperature and precipitation variables, producing trend and p-value maps for each variable. All trends were scaled from annual values to decadal values (*i.e.,* by multiplying by 10) and reported as means (± one standard deviation)/decade in the appropriate units. For instance, SOS trends were expressed in days/decade and temperature trends in °C/decade.

For a complementary analysis of trends, we employed the seasonal trend analysis (STA) tool within the Earth Trend Modeler. STA is based on detection of the within-year seasonal cycles; therefore, the three-day EVI2 time series was used instead of the annual time series of phenometrics. Each year of data was first submitted to a harmonic regression to produce five shape parameters based on sine functions, which characterize the seasonal cycles of that year at each specific location/pixel. The five shape parameters are: (1) Amplitude 0, the annual mean EVI2 value; (2) Amplitude 1, the amplitude of the annual cycle; (3) Amplitude 2, the amplitude of a semiannual cycle; (4) Phase 1, the location (in phase angle) of the beginning of the series on the annual cycle; and (5) Phase 2, the location of the beginning of series on a semiannual cycle. A Theil-Sen median trend analysis was then run on each shape parameter time series over the study period. The resultant trend images for the five shape parameters along with the corresponding p-value maps were then evaluated separately.

We also assessed the impact of seasonal temperature and precipitation on the phenometrics using partial correlation analysis. Partial correlation measured the association between a phenometric and a seasonal climate variable when the effects of other variables were removed. For SOS, prior winter (NDJ) temperature and precipitation, and spring (FMA) temperature and precipitation were used as predictor variables. For EOS, prior summer (MJJ) temperature and precipitation, and autumn (ASO) temperature and precipitation were used. A partial correlation map was produced for each pair of phenometric and climate variable. We computed the p-values of the partial correlation coefficients for each map following a Clark Labs support article (https://forums.clarklabs.org/hc/en-us/articles/207103527-Procedures-for-Testing-the-Significance-of-a-Linear-Model-using-ETM).

Regional analysis of the detected trends

The detected trends were subsequently analyzed and reported by the 17 NEON domains that partition CONUS (Table 1, Figure 1). To facilitate areal comparisons, all trend images were projected to an Albers Equal Area Conic coordinate system. We focused on the statistically significant ($p<0.05$) trends and evaluated their directions, percentage areas, and magnitudes in each NEON domain. Specifically, zonal statistics were computed for the significant trends in the three phenometrics (SOS, EOS, and GSL), the five harmonic-regression-based shape parameters (Amplitude 0, Amplitude 1, Amplitude 2, Phase 1, and Phase 2), and the seasonal climatic variables for every NEON domain within CONUS.

To evaluate the predominance of the direction of a trend within a region, we calculated an asymmetry ratio (AR) of the area of a significant negative trend to the area of the significant positive trend (Tomaszewska and Henebry 2018, Tomaszewska *et al.* 2020) for each variable. We set two thresholds to interpret the AR values: if the AR value was greater than 2.0 (or less than 0.5), it indicated that there was a predominant significant negative (or positive) trend associated with a given variable within the domain of interest. An AR value between 0.5 and 2.0 can be interpreted as indicating mixed or neutral trends, including the occurrence of expected randomly distributed false positives and negatives. Further, to evaluate the degree of variation in trend magnitudes, we calculated coefficients of variation (CV, calculated as 100×standard deviation/mean, in %) for each NEON domain and over the entire CONUS.

In addition, STA allowed for simulation of the annual EVI2 curves at the beginning and the end of the study period based on the detected trends of the five harmonic regression parameters. We produced a reconstructed EVI2 curve for the beginning two years (1982-1983) and another curve for the ending two years (2015-2016) of the study period to show changes for each NEON domain. We further identified the primary land use / land cover types of the areas with significant trends in the phenometrics and harmonic regression parameters in reference to the 2016 MODIS IGBP land cover classes. Finally, we employed the same zonal statistics approach to assess the different directions and degrees of partial correlations between phenometrics and seasonal climate variables by NEON domains. The AR analysis was also applied to evaluate the predominant directionality of the partial correlations.

Results

Overview

Different NEON domains exhibited various directions, magnitudes, and prevalence of trends in the three phenometrics: SOS (Figure 1a), EOS (Figure 1b), and GSL (Figure 1c). Areal percentages of significant ($p<0.05$) trends with summary statistics of their magnitudes with respect to NEON domains are provided in Table 1 for SOS, Table 2 for EOS, and Table 3 for GSL. A pairwise visualization of the directions and areal percentages of predominant ($AR<0.5$ or $AR>2$) significant ($p<0.05$) changes in the phenometrics serves as a summary of the phenological changes in different NEON domains (Figure 2). Significant ($p<0.05$) partial correlations of the seasonal climatic variables with SOS / EOS (Figure S1, in the Appendix S1) and the significant ($p<0.05$) trends in the seasonal climatic variables (Figure S2) demonstrated spatial variations that are coherent with those of the phenological trends (details to follow). Predominant partial correlations between SOS / EOS and seasonal climatic variables and trends (directions and areal percentages) in seasonal climatic variables by NEON domains are summarized in the bivariate charts in Figures 3 and 4, respectively. Detailed statistics of the partial correlations between SOS/EOS and climatic variables and seasonal climatic trends by NEON domains are available in supplemental tables (Tables S1-S16, Appendix S1). Land use / land cover areal percentage contributions to predominant trends in phenometrics by NEON domains further revealed potential underlying causes of phenological changes, especially in relation to agriculture (Figure 5). Detailed statistics of the contributions of land use / land cover to significant trends in the phenometrics by NEON domains are available in supplemental Tables S17-S19. The areal percentage contributions of respective land use / land cover types to the predominant changes in phenometrics across CONUS are provided in Table 4.

Trends in harmonic regression parameters showed additional details of the regional patterns of phenological change (Figure 6, Tables S20-S29). Units for the magnitudes of trends in the harmonic regression parameters, such as EVI2 ratio/decade for annual mean EVI2 (Amplitude 0), annual amplitude (Amplitude 1) and semiannual amplitude (Amplitude 2) and °/decade for annual phase (Phase 1) and semiannual phase (Phase 2), do not carry direct biophysical interpretations, but rather indicate changes in seasonal vegetation indirectly. Therefore, we focus on reporting the directions of the trends in the harmonic regression parameters. Increased EVI2 values and amplitudes are generally associated with increases in land surface greenness and productivity. Changes in the phase parameters reflect shifts in the sinusoidal curves used to simulate EVI2 annual trajectories over the study period. A positive trend in phase angles generally indicates an earlier shift of growing season / cycle (annual or semiannual) and a negative trend a later shift of growing season / cycle. In addition to regional patterns of the trends in respective parameters, reconstructed annual EVI2 curves at the beginning and the end of the study period (1982-2016) demonstrated overall trends of the entire growing seasons averaged across each NEON domain (Figure 7).

Below we emphasize the continental scale trends across the NEON domains and over the entire CONUS. The specific results with respect to each NEON domain are provided in Appendix S1, which also contains the supplemental tables and figures. In the appendix, the results and discussion for the NEON domain 1 (Northeast) is covered in more detail to set up the template for subsequent domains. However, the remaining domains are described more concisely, focusing on the significant, predominant, and widespread trends and relationships, while the full details for each domain are available in the corresponding figures and tables. For readers who would like to explore detailed domain-specific patterns, please refer to the Appendix S1 and associated raster layers of analysis results in the Data S1 and Data S2. Unless otherwise noted, all trends and correlations reported in the main text and the supplemental document are statistically significant ($p<0.05$).

Overall domain-level patterns in phenometrics

SOS has become predominantly later by varied areal extents in most NEON domains, except for Northern Rockies (12), Great Basin (15), and Pacific Southwest (17) where significant trends did not display a predominant pattern, and for Pacific Northwest (16) where SOS has become predominantly earlier (Table 1, Figures 1a and 2a). EOS became predominantly later in nine domains (1-3, 5, 8, 11-14), and earlier in three domains: Prairie Peninsula (6), Central Plains (10) and Atlantic Neotropical (4), with the remaining five domains showed no predominance in significant trends (Table 2, Figures 1b and 2b). Accordingly, for the eleven domains with predominant significant trends found in both spring and autumn phenometrics, eight (1-3, 5, 8, 11, 13, 14) occurred later in both SOS and EOS, and three (4, 6, 10) occurred later in SOS and earlier in EOS (Figure 2c). The remaining six NEON domains (7, 9, 12, 15-17) exhibited a predominant significant trend in one of the phenometrics or neither.

Consequently, GSL predominantly shortened in eleven domains (2-6, 8-11, 14, 15) in varied areal percentages (Table 3, Figures 1c, 2a and 2b). In Prairie Peninsula (6), Central Plains (10) and Atlantic Neotropical (4), this shortening trend clearly corresponded with later SOS and earlier EOS. Among other domains with predominant trends of shortened GSL, four scenarios can be identified (Tables 1-3, Figures 2a and 2b). First, a pattern of *more later/later,* in which both SOS and EOS occurred predominantly later but the area of later SOS surpassed that of later EOS, appeared in five domains: Mid Atlantic (2), Southeast (3), Ozarks Complex (8), Southern Plains (11), and Desert Southwest (14). The second pattern *lot later/little later* appeared only in Great Lakes (5), where both SOS and EOS occurred predominantly later and the area of later SOS (19.0%) was slightly smaller than that of later EOS (23.4%), but the magnitudes of later SOS (5±4 days/decade) were greater than that of later EOS (3±2 days/decade). A third pattern *later/mixed* was found in Northern Plains (9), where SOS occurred predominantly later, but EOS showed mixed opposing trends of earliness (11.9%, -5±6 days/decade) and lateness (12.8%, 5±6 days/decade). A fourth pattern *mixed/lot earlier* was found in Great Basin (15): SOS trends were mixed but earlier in more areas (12.1%, -4±3 days/decade *vs.* 6.2%, 5±4 days/decade) and EOS occurred both later (16.8%, 5±4 days/decade) and earlier (13.3%, -10±6 days/decade) but the magnitudes of EOS becoming earlier were double those of other significant trends. Finally, GSL became predominantly longer only in two domains on opposite coasts: Northeast (1) and Pacific Northwest (16).

Climate associations with SOS and EOS and trends in the seasonal climate variables also varied across NEON domains (Figures 3, 4, S1, and S2). Winter temperatures mostly showed few or non-predominant partial correlations with SOS at the domain scale (Figure 3a) but increased predominantly over large extents in most western domains (Figure 4a). Spring temperatures were predominantly negatively correlated with SOS (warmer spring→earlier SOS) in most domains except Pacific Southwest (17) and Desert Southwest (14) (Figure 3a). Spring temperatures predominantly increased in most western domains (10-17) but only slightly (1%) in Southeast (3) and it either decreased or was not predominant in other eastern domains (1-2, 4-9) (Figure 4a). Across all domains, winter precipitation showed few (smaller percentage areas) or no predominant partial correlations with SOS (Figure 3c), and few or no predominant significant changes during the study period (Figure 4c). Spring precipitation increased extensively in Great Lakes (5) and decreased extensively in Southern Rockies (13) and Desert Southwest (14) (Figure 4c). Among these three domains with more extensive changes, spring precipitation was predominantly positively correlated with SOS (more precipitation→later SOS) in Great Lakes (5), but negatively correlated with SOS (more precipitation→earlier SOS) in Southern Rockies (13) and Desert Southwest (14, Figure 3c). Predominant negative correlations between summer temperatures and EOS were more extensive in Northeast (1) and Great Lakes (5); predominant positive correlations appeared in Southern Rockies (13) and Southeast (3); other domains showed relatively small areas of partial correlations or no areal predominance (Figure 3b). Majority of the domains (1-3, 5, 7, 8, 11, 13, 15) showed predominant positive correlations of autumn temperatures with EOS, whereas Prairie Peninsula (6), Northern Plains (9), and Pacific

Northwest (16) showed negative correlations. Five other domains (4, 10, 12, 14, 17) showed no predominant significant correlations of EOS with autumn temperatures. A near dual trend of increased summer and autumn temperatures is evident across nearly every domain (Figure 4b). The sole exception is Northern Plains (9) where summer temperatures predominantly decreased in a small area of the domain. Partial correlations of EOS with summer precipitation exhibited more complicated patterns; and partial correlations of EOS with autumn precipitation showed positive correlations in all eastern and plains domains (1-11) and no predominant correlations in all western domains (12-17) (Figure 3d). Summer precipitation increased in all eastern and plains domains (1-11), as well as slightly in Desert Southwest (14), but decreased in the other western domains (12, 13, 15-17) (Figure 4d). Autumn precipitation mostly increased in the eastern domains along the Atlantic Coast (1-4, 7), Northern and Central Plains (9,10), and Pacific Northwest (16), but decreased over relatively large areas in Southern Rockies (13) and Desert Southwest (14).

Predominant trends in phenometrics were associated with either croplands or various natural vegetation cover types, depending on the domain (Figure 5). The contribution of croplands to the significant changes in phenometrics was centered around Prairie Peninsula (6) and extending to neighboring domains. Majority of the predominantly significant trends in all three phenometrics in Prairie Peninsula (6) occurred in croplands. In addition, croplands contributed substantially to predominantly significant SOS trends (Figure 5a) in Great Lakes (5), Appalachians / Cumberland Plateau (7), Ozark Complex (8), Northern Plains (9), and Central Plains (10), to predominantly significant EOS trends (Figure 5b) in Central Plains (10), and to predominant significant GSL trends (Figure 5c) in Great Lakes (5), Mid Atlantic (2), Ozark Complex (8), Southeast (3), Northern Plains (9), and Central Plains (10).

CONUS-level patterns in phenometrics

Across CONUS, later trends in SOS (7±5 days/decade, Table 1) were predominantly significant (24.3%) over earlier trends (3.6%; -5±4 days/decade). Later occurrences of SOS were mainly found over croplands (35.9%) and grasslands (33.4%) in central and eastern parts of CONUS; while earlier occurrences of SOS were more concentrated over natural vegetation covers (grasslands=45.2% and evergreen needleleaf forests =22.0%) in the northwestern CONUS (Figures 1a and 2a, Table 4). In both winter and spring, significant temperature increases occurred (13.0%, 0.60±0.21°C/decade and 7.2%, 0.50±0.14°C/decade, respectively) primarily in the western CONUS (Figures 4a, S2a, Tables S2 and S6). Spring temperature was the only climatic variable that showed widespread (24.2%) and significant (negative) correlations with SOS across most part of CONUS, except the desert southwest (Figures 3 and S1, Tables S1, S3, S5, and S7). Although mixed in direction and minimal in area at the scale of CONUS, negative correlations of spring precipitation with SOS (increased spring precipitation➔ earlier SOS) were common in the desert southwest (Figures 3c and S1d, Table S7), where significant decreases in spring precipitation also occurred more than anywhere else (Figures 4c and S2d, Table S8).

EOS occurred both earlier (-7±5 days/decade, 10.6%) and later (5±3 days/decade, 14.1%) in various parts of CONUS (Figure 1b, Table 2). Earlier occurrences of EOS appeared mostly over croplands (66.8%) and grasslands (23.3%, Table 4) and appeared to be concentrated in the farmlands of the Midwest and a portion of the Great Basin. In contrast, later EOS occurred mainly over natural vegetation covers such as grasslands (36.7%) and woody savannas (22.7%). Summer and autumn temperatures both increased widely (0.39±0.12°C/decade, 24.9%; 0.40±0.12°C/decade, 35.8%, respectively) across CONUS, except a large region centered in the Midwest (Figures S2e and S2g, Tables S10 and S14). In addition, temperature increases in both summer and autumn were greater in magnitudes in the West compared to the East, with more areas in the West showing increased trends of >0.5°C/decade. Summer precipitation exhibited predominantly significant increases (33±8 mm/decade, 6.3%) in the northeastern and midwestern CONUS, but decreased in small patches (1.0%) in the West (Figure S2f, Table S12). Similarly, autumn precipitation predominantly increased (29±12 mm/decade) in central and eastern CONUS (5.2%, Table S16) but decreased in small clustered areas (1.8%) in the desert southwest (Figure S2h). Despite the trends in summer variables, no predominant or widespread correlations were found between summer temperatures and precipitation with EOS at the CONUS level (Tables S9 and S11). Predominantly significant positive correlations (5.3%) were found between autumn temperature and EOS, especially in regions away from the farmlands of the midwestern CONUS (Figure S1g, Table S13). Although restricted to small areas (3.2%), autumn precipitation was predominantly and positively correlated with EOS (Table S15). Finally, GSL was predominantly significantly shortened (-14±9 days/decade, 20.5%, Table 3) over croplands (48.9%) and grasslands (37.9%) across CONUS (Table 4). Whereas, in 6.2% of CONUS, GSL was significantly lengthened (8±6 days/decade) mainly over natural vegetation types: grasslands (33.9%) and woody savannas (17.1%).

From an alternative perspective, evergreen needleleaf forest was the only land cover category in which predominantly earlier significant SOS trends (61,192 km^2) occurred; whereas, in all other land cover categories predominantly later significant SOS trends occurred (Table 4). Predominantly significant earlier EOS trends occurred most extensively in croplands (548,227 km^2) and to a much lesser extent in closed shrublands (1,655 km^2). Most other land cover types exhibited predominantly later EOS trends, most extensively in grasslands (400,519 km^2) and woody savannas (247,961 km^2). Predominantly significant shorter GSL trends occurred most extensively in croplands (776,295 km^2) and grasslands (602,042 km^2). In contrast, predominantly longer GSL occurred most extensively in evergreen needleleaf forests (77,194 km^2) and deciduous broadleaf forests (37,755 km^2).

Change in STA across NEON domains and CONUS

Trends of significant increases were predominant in annual mean EVI2 (63.7%), annual amplitude (51.6%), and semiannual amplitude (42.2%) across CONUS (Tables S20, S22, S24). The increasing trends of these three parameters were particularly attributed to grasslands (45.1%, 35.8%, and 42.3%, respectively) and croplands (19.5%, 28%, and 34.1%, Tables S21, S23, S25, respectively). Significant increases of annual mean EVI2 predominated in most domains and particularly in the Plains domains (9-11) and Southeast (3, Figure 6a). Exceptions were clustered regions of significant decreasing trends in the Northeast (1) and parts of the eastern and midwestern domains (5-7, Figure 6a). Similarly, significant increases in annual amplitude were also predominant in most NEON domains and were especially distinctive in Prairie Peninsula (6) and the Plains domains (9-11, Figure 6c). Areas with significant increases in semiannual amplitude particularly mirrored the nation’s agricultural zones in Prairie Peninsula (6), Northern Plains (9), Central Plains (10), and the Lower Mississippi River Valley within Ozarks Complex (8) (Figure 6e). Negative trends in annual phase angle in association with a later shift of growing season were predominant (21.2%) over positive trends (6.8%) across CONUS (Table S26). Areas of negative trends (later shifts) in annual phase angle were mainly in eastern CONUS with relatively small magnitudes of change except a portion in the desert southwest, whereas, significant positive trends (earlier shifts) were concentrated in western CONUS (Figure 6b). Both the negative and positive trends in annual phase angles were primarily attributed to grasslands (30.9% and 54.7%, respectively) and croplands (21.5% and 12.5%, respectively, Table S27). The trends in semiannual phase angle were mixed at the CONUS level (Table S28), with negative (later shift) trends (11%) associated with croplands (34.1%) and grasslands (22.7%) and positive (earlier shift) trends (12.5%) with grasslands (46.1%) and open shrublands (13.1%, Table S29). A similar east-west contrast appeared in the geographic distribution of significant trends in semiannual phase, except that higher magnitudes of negative trends were found in the Great Plains (Figure 6d). Referencing the domain-specific reconstructed EVI2 curves, every domain exhibited increased EVI2 either within parts or throughout the growing seasons (Figure 7). A visual comparison of the reconstructed EVI2 curves suggested that the magnitudes of the EVI2 increases were smaller and focused during the peak of the growing seasons in the East (1-8), but were greater in magnitude and distributed across the annual cycle in the West (9-17)

Discussion

Across the NEON domains, specific trends in LSP phenometrics demonstrated geographic patterns that are coupled with regional ecoclimatic characteristics, climate change trends, and land use / land cover differences. An apparent climatic and ecological dipole (Zuckerberg *et al.* 2020) between western and eastern CONUS was highlighted in our findings. Besides the stark physiographic differences between the two broad regions, significant warming also occurred mainly in the West but was absent in a large portion of the East, especially during winter and spring (Figures 3 and S2). This difference in climatic trends concurs with studies using weather records over the past century that showed a lack of warming trend in the southeastern U.S. (*e.g.*, Rogers 2013, Gil-Alana and Sauci 2019). In response to the more pronounced warming in the western U.S., significantly earlier SOS was found in the humid Northwest, especially in Pacific Northwest (16)—although the area of significant spring temperature increase was small—and the northern part of Great Basin (15) (Figures 1a, 4a, S2a and S2c). In contrast, SOS shifted predominantly later in the drier Southwest, apparently due to reduced spring precipitation (Figures 3c, 4c, S1d and S2d). As the primary cover type associated with earlier SOS in Pacific Northwest was Evergreen Needleleaf Forest, it is likely that the observed phenological changes were contributed substantially by understory growth. The understory vegetation may also have become more visible due to tree mortality from mountain pine beetle and spruce budworm outbreaks in the region (Meigs *et al.* 2015). The warming-induced earlier SOS trends were more fragmented in spatial distribution and complicated by the diverse topo-climatic landscapes and vegetation community types in Northern Rockies (12) and Pacific Southwest (17). McCabe *et al.* (2012) demonstrated a similar northwest-southeast dipole in both the trends of modelled first leaf dates during the 1900-2008 period and the corresponding spatial pattern of spring temperature anomalies during positive phases of El Niño/Southern Oscillation (ENSO) and Pacific Decadal Oscillation (PDO). Over most part of the eastern CONUS, SOS has become predominantly later, especially in domains that overlap with the agricultural belts of the U.S. as supported by the large portions of croplands that contributed to the later trends in SOS (Figure 1a, Table 4). The later shift in SOS there may likely be controlled by changes in agronomic practices, *viz.*, cultivation of different crop varieties, changes in tillage practices, and shifts to later-emerging crops (corn and soybean) over earlier-emerging crops (winter wheat and oats) (*cf.* Zhang *et al.* 2019).

Similarly, trends in EOS were also influenced by both seasonal climate and land use / land cover changes. Predominant later trends in EOS occurred primarily over natural vegetation types with warmer autumn temperatures as the primary driver, across a number of both eastern and western domains (1-3, 5, 8, 11, and 13, Figures 1b, 2b, 3b and 4b, Tables 2 and 4). While earlier EOS was mostly found over croplands, especially within the agricultural lands that are centered in Prairie Peninsula (6), where significant autumn warming was not apparent. Instead, the earlier EOS over agricultural lands was likely caused by earlier crop harvesting: Sacks and Kucharik (2011) showed trends of earlier harvesting dates of both corn and soybean in the Midwestern Corn Belt from 1981 to 2005 due to shorter dry-down time after maturity. Therefore, both the absence of significant autumn warming and changes in crop management practices may have contributed to earlier EOS in the agriculture-intensive domains (6, 10). In addition, a positive relationship of later EOS with increased autumn precipitation (Figure S1h) was predominant in every central and eastern domain (1-11), while all other domains in the west (12-17) showed mixed relationships, albeit all in small areas (Table S15). Therefore, in addition to warmer autumn temperatures, later EOS in certain non-agricultural domains such as Northeast (1) and Mid Atlantic (2) may arise, in part, from increased autumn precipitation (Figures S1h and S2h, Table S16).

Shortened GSL due to later SOS and earlier EOS in agricultural heartland of Prairie Peninsula (6) and Central Plains (10) (Figure 1c) matched the distribution of the similar trend patterns found by Garonna *et al.* (2016). About 48.9% of the shortened GSL was associated with croplands as constrained by later SOS and earlier EOS from changing agricultural practices (Table 4). Only two domains—Northeast (1) and Pacific Northwest (16) exhibited predominantly significant trends of extended GSL (Table 3). In Northeast, areas with predominantly later EOS (14.4%, 60,875 km^2) exceeded that of later SOS (5.0%, 21,200 km^2), hence the prolonged GSL was primarily caused by strong autumn warming (Figures 3b and 4b, Tables 1 and 2). In Pacific Northwest, GSL extension corresponded with predominantly earlier SOS (27.7%, Table 1), along with more area of later EOS (17.5%, Table 2) than earlier EOS (10.2%), though not predominantly greater. These significant trends of extended GSL in both

Northeast and Pacific Northwest were both associated with natural vegetation cover types (Table S19) and were primarily caused by climate driven shifts in SOS and EOS.

The varied climatic effects on SOS and EOS respectively can be further understood in light of the seasonality and geographic distribution of the region exhibiting no significant warming trend in eastern CONUS, also known as the U.S. Warming Hole (Mascioli *et al.* 2017, Partridge *et al.* 2018). Partridge *et al.* (2018) showed that over the period from 1961 to 2015, the Warming Hole—characterized by regional cooling—was persistently positioned over the southeastern U.S. during winter (DJF) and spring (MAM), and over the midwestern U.S. during summer (JJA) and autumn (SON). Similar regional patterns of seasonal temperature trends were also demonstrated using monthly accumulated growing degree-days over CONUS (Kukal and Irmak 2018). This seasonal variation of the location of the Warming Hole agrees, in part, with the geographic patterns of seasonal temperature trends we detected over a shorter period from 1982 to 2016 (*cf.* Figure S2). We used a different division of months into seasons (*e.g.*, FMA=spring) to account for plant phenological responses to prior weather conditions. In spite of these differences, both our results and Partridge *et al.* (2018) suggested that the winter-to-spring Warming Hole over much of the eastern U.S. covered by natural vegetation may have inhibited an earlier trend in spring phenology that would otherwise be anticipated as a consequence of climatic warming. On the other hand, the summer-to-autumn Warming Hole overlapped more with the agricultural zones in the midwestern U.S. with the effect of cooler temperature being largely overridden by changes in agricultural practice, especially in Prairie Peninsula (6), Central Plains (10) and the Lower Mississippi River Valley within Ozarks Complex (8). Yet in other eastern CONUS domains covered mostly by natural vegetation (1-3, 5, and 8), we found predominantly later EOS as expected from the effect of warmer autumn temperatures.

Additional details of LSP change as revealed by the seasonal trend analysis (STA) suggested an overall increase of greenness and productivity throughout the vegetated land surfaces in CONUS over the past three decades. A recent study showed similar greenness increases over both croplands and natural vegetation covers in Americas based on MODIS collection 6 NDVI and EVI products (Heck *et al.* 2019). The varied spatial patterns of trends using three different amplitudes of harmonic regression curves revealed that while increases in annual average EVI2 occurred over both natural vegetation and croplands, the increases in annual amplitude and semiannual amplitude were more associated with croplands (Figure 6 and Tables S21, S23, S25). Given that semiannual amplitude is a modifying factor to the annual curves reconstructed by harmonic regression, its positive trend and geographic pattern revealed increased growth and productivity of croplands in the domains of the agricultural heartland, Prairie Peninsula (6), Northern Plains (9) and Central Plains (10) (Figure 6e, Figure 7). While greening of vegetation can be generally attributed to rising temperature and CO_2 fertilization in the context of global climate change (Los 2013, Zhu et al. 2016), significantly increased productivity in the agricultural lands may be more contributed by technological improvements and innovations (Lobell and Asner 2003, Fuglie 2007, Wang *et al.* 2015, Zhang *et al.* 2019). In addition, the observed vegetation productivity increases in the Upper Midwest may also arise from relatively recent land use changes, such as conversion of native grasslands and wetlands to croplands (Johnston 2013, Wright and Wimberly 2013, Johnston 2014, Lark *et al.* 2015, Johnston and McIntyre 2019, Lark *et al.* 2019). Earlier shift of annual growing cycles (increased annual phase angles) over natural vegetation in Great Basin (15) , Pacific Northwest (16), and

Pacific Southwest (17) (Figures 6b and 6d) appeared to correspond, in part, with earlier SOS in those domains influenced by climate warming. Moreover, due to a lack of widespread influence from changes of both climate and agriculture, the forested domains in the eastern CONUS, such as Northeast (1), Mid Atlantic (2), Great Lakes (5), and Appalachians / Cumberland Plateau (7) showed relatively smaller changes in the averaged seasonal EVI2 profiles in comparison to other domains (Figure 7). The slight increases of greenness during the peaks of growing seasons in these largely forested domains may be partly explained by increased summer precipitation (Figure S2f) and/or increased forest aboveground biomass densities (Oswalt *et al.* 2019).

Using NEON domains as a spatial framework, our study has demonstrated close relationships between long-term changes in LSP and the underlying drivers in a regionally explicit context. The sensitivity of phenology to environmental changes and the ecoclimatic consistency in its variability in time and space offer an important perspective to investigating vegetation changes and ecoregion differences (Morisette *et al.* 2009, Weltzin *et al.* 2020). This idea has been embodied in previous studies using satellite-derived information to delineate phenologically similar regions (Loveland *et al.* 1995, White *et al.* 2005a, Bradley and Mustard 2008, Brooks et al. 2020). For instance, our study highlighted the variable LSP responses across regions that are dominated by either natural or managed vegetation systems. Underlying broad land use / land cover patterns, land surface phenology is further influenced by finer environmental gradients and natural disturbances to vegetation and disturbance history at the regional scales (Norman *et al.* 2017). On the other hand, since LSP signals vary from year to year due to interannual climatic fluctuations and recent weather, phenoregions derived therein may have limited ability to reveal inherent vegetation changes arising from changes in land use / land cover, ecological succession, disturbances, and invasive species, as well as slower onset aspects of climate change. One approach to solving this problem is by standardizing LSP using climate-driven phenological models to attenuate the effect of interannual climate fluctuations and thereby accentuate intrinsic vegetation properties and/or differences in land use / land cover (Liang *et al.* 2016). In the current study, we utilized long-term trends in LSP to highlight the portion of differences in satellite observations that are associated with regional vegetation growth differences by linking explicitly the observed trends to regional changes in land use / land cover and seasonal climate.

Identifying regional trends in phenology within different NEON domains in relation to their corresponding drivers should facilitate annual and seasonal planning in anticipatory natural resource management according to domain-specific climate change and land change patterns (Bradford *et al.* 2018). Given potential large changes in both composition and structure of terrestrial ecosystems under climate change (Nolan *et al.* 2018), consistent monitoring of the coupled changes of ecosystems and climate are essential for successful implementation of climate adaptation plans. NEON is equipped with a network of Terrestrial Observation Systems (Thorpe *et al.* 2016) complete with consistent protocols for ground-level observation of phenological variables (Elmendorf *et al.* 2016) and complemented by periodic airborne remote sensing designed to reveal disturbances and short-term changes (Kampe 2010). Yet, inference from a sparse set of observations to domain understanding requires knowledge of recent significant changes, *viz.*, *trends* properly understood, that have occurred within the domain. Therefore, ongoing efforts are needed to keep track of the changes, anomalies, trends, and trend changes in land surface phenology within regionally specific context of the NEON domains. Furthermore, we would argue that it is an opportune time to evaluate the representativeness of the NEON core sites in providing reference conditions for phenological and ecological changes that have occurred within the domain. A first step is to compare the distribution of detected LSP trends at each domain with local observations at the respective core sites. The NEON relocatable intensive measurement capabilities could play a role in addressing discrepancies between core sites and domain predominant phenological trends.

Finally, using LSP and NEON domains as an underlying spatial framework, results from this study and further research along this line can provide a means through which to collaborate with other distributed observatory networks, such as Long Term Ecological Research Network (LTER), Long-Term Agroecosystem Research Network (LTAR), FLUXNET, and the citizen science based USA-National Phenology Network (USA-NPN). Given that these networks aim to collect relevant environmental information from discrete field sites, the LSP observations derived from wall-to-wall spatial coverage could serve as the foundation from which to interpolate and integrate site-level information to broader scale generalizations. Since ground level phenological observations require no specialized or costly equipment, just some training and a modicum of repeated observational effort (Leopard and Jones 1947; Crimmins *et al.* 2017), these networks can leverage ecological monitoring to support continental scale forecasting tasks. The site level observations and measurements within these networks will, in turn, contribute to elucidating the underlying processes and drivers of satellite detected changes and, when compared across sites and domains, help achieve multi-scale understanding of the status and trends of ecosystems and landscapes across CONUS.

Conclusion

In this study, we found that the regional patterns of long-term (1982-2016) trends in land surface phenology across National Ecological Observatory Network (NEON) domains in the conterminous United States (CONUS) closely followed the underlying geographies of seasonal climate change, land use / land cover dynamics, and regional vegetation differences. Warming-induced earlier SOS mainly occurred in the northwestern domains such as Pacific Northwest (16); whereas, in the midwestern domains, such as Prairie Peninsula (6), later SOS timing was predominant due both to a lack of warming in spring and recent changes in agricultural practices. In contrast, EOS timing has become later in most NEON domains covered with natural vegetation in response to a more widespread autumn warming. However, earlier EOS was predominant in the domains with extensive agricultural lands likely due to earlier crop harvesting. Accordingly, while trends of prolonged GSL were mostly found over natural vegetation in domains that were more affected by climate change, such as Pacific Northwest (16) and Northeast (1), shortening trends in GSL were more commonly related to land management changes in domains that are covered by extensive agriculture. During the study period, natural vegetation has become "greener" in most NEON domains due potentially to factors such as warmer temperatures, increased precipitation, conversion of grasslands and wetlands to croplands, including agroforestry plantations, as well as ecological succession and/or invasive species, with variable relative importance in these factors across the domains. The crop productivity in agriculture-intensive domains has also increased due to improved farming technologies, crop varieties, and agronomic practices. Spatial details of the domain-specific LSP trends and their associated climatic drivers provide a useful domain-wide reference to the ongoing phenological, ecological, climatological, and cross-scale observations at the NEON terrestrial field sites and other distributed observatory networks. The supplemental online materials (https://doi.org/10.13023/kjn2-p817) provide detailed results by NEON domain as well as the raster data documenting the phenological trends.

Acknowledgements:

LL would like to thank the College of Arts & Sciences, University of Kentucky for supporting his sabbatical leave, and the Geospatial Sciences Center of Excellence at SDSU for hosting a semester-long visit that led to the current collaborative research. This work was partially supported by grant NNX14AJ32G to GMH, and grant 80NSSC18K0626 to XYZ. We also thank the two anonymous reviewers for their helpful and constructive comments.

References

Bradford, J. B., J. L. Betancourt, B. J. Butterfield, S. M. Munson, and T. E. Wood. 2018. Anticipatory natural resource science and management for a changing future. Frontiers in Ecology and the Environment **16**:295-303.

Bradley, B. A., and J. F. Mustard. 2008. Comparison of phenology trends by land cover class: A case study in the Great Basin, USA. Global Change Biology **14**:334-346.

Brooks, B.-G. J., D. C. Lee, L. Y. Pomara, and W. W. Hargrove. 2020. monitoring broadscale vegetational diversity and change across North American landscapes using land surface phenology. Forests **11**:606.

Chmura, H. E., H. M. Kharouba, J. Ashander, S. M. Ehlman, E. B. Rivest, and L. H. Yang. 2019. The mechanisms of phenology: the patterns and processes of phenological shifts. Ecological Monographs **89**:e01337.

Cleland, E. E., I. Chuine, A. Menzel, H. A. Mooney, and M. D. Schwartz. 2007. Shifting plant phenology in response to global change. Trends in Ecology & Evolution **22**:357-365.

Collinge, S. K. 2018. NEON is your observatory. Frontiers in Ecology **16**:371.

Crimmins, T.M., Crimmins, M.A., Gerst, K.L., Rosemartin, A.H. and Weltzin, J.F., 2017. USA National Phenology Network's volunteer-contributed observations yield predictive models of phenological transitions. PLoS One **12**:e0182919.

de Beurs, K. M., and G. M. Henebry. 2004. Land surface phenology, climatic variation, and institutional change: Analyzing agricultural land cover change in Kazakhstan. Remote Sensing of Environment **89**:497-509.

de Beurs, K. M., and G. M. Henebry. 2010. Spatio-temporal statistical methods for modelling land surface phenology. Pages 177-208 Phenological Research: Methods for Environmental and Climate Change Analysis.

Eastman, J. R., F. Sangermano, B. Ghimire, H. Zhu, H. Chen, N. Neeti, Y. Cai, E. A. Machado, and S. C. Crema. 2009. Seasonal trend analysis of image time series. International Journal of Remote Sensing **30**:2721-2726.

Elmendorf, S. C., K. D. Jones, B. I. Cook, J. M. Diez, C. A. F. Enquist, R. A. Hufft, M. O. Jones, S. J. Mazer, A. J. Miller-Rushing, D. J. P. Moore, M. D. Schwartz, and J. F. Weltzin. 2016. The plant phenology monitoring design for the national ecological observatory network. Ecosphere **7(4)**:1-16.

Fuglie, K. O. 2007. Productivity growth in US agriculture. US Department of Agriculture, Economic Research Service.

Garonna, I., R. de Jong, and M. E. Schaepman. 2016. Variability and evolution of global land surface phenology over the past three decades (1982–2012). Global Change Biology **22**:1456-1468.

Gil-Alana, L. A., and L. Sauci. 2019. US temperatures: Time trends and persistence. International Journal of Climatology **39**:5091-5103.

Heck, E., K. M. de Beurs, B. C. Owsley, and G. M. Henebry. 2019. Evaluation of the MODIS collections 5 and 6 for change analysis of vegetation and land surface temperature dynamics in North and South America. ISPRS Journal of Photogrammetry and Remote Sensing **156**:121-134.

Henebry, G. M., and K. M. de Beurs. 2013. Remote sensing of land surface phenology: A prospectus. Pages 385-411 Phenology: An Integrative Environmental Science. Springer.

Hoaglin, D. C., F. Mosteller, and J. W. Tukey. 2000. Understanding robust and exploratory data analysis.

Huete, A. R., K. Didan, Y. E. Shimabukuro, P. Ratana, S. R. Saleska, L. R. Hutyra, W. Yang, R. R. Nemani, and R. Myneni. 2006. Amazon rainforests green‐up with sunlight in dry season. Geophysical Research Letters **33**:L06405.

Jiang, Z., A. R. Huete, K. Didan, and T. Miura. 2008. Development of a two-band enhanced vegetation index without a blue band. Remote Sensing of Environment **112**:3833-3845.

Johnston, C. A. 2013. Wetland losses due to row crop expansion in the Dakota Prairie Pothole Region. Wetlands **33**:175-182.

Johnston, C. A. 2014. Agricultural expansion: land use shell game in the US Northern Plains. Landscape Ecology **29**:81-95.

Johnston, C. A., and N. E. McIntyre. 2019. Effects of cropland encroachment on prairie pothole wetlands: numbers, density, size, shape, and structural connectivity. Landscape Ecology **34**:827-841.

Julien, Y., and J. Sobrino. 2009. Global land surface phenology trends from GIMMS database. International Journal of Remote Sensing **30**:3495-3513.

Justice, C., B. Holben, and M. Gwynne. 1986. Monitoring East African vegetation using AVHRR data. International Journal of Remote Sensing **7**:1453-1474.

Justice, C. O., E. Vermote, J. R. G. Townshend, R. Defries, D. P. Roy, D. K. Hall, V. V. Salomonson, J. L. Privette, G. Riggs, A. Strahler, W. Lucht, R. B. Myneni, Y. Knyazikhin, S. W. Running, R. R. Nemani, Z. M. Wan, A. R. Huete, W. van Leeuwen, R. E. Wolfe, L. Giglio, J. P. Muller, P. Lewis, and M. J. Barnsley. 1998. The Moderate Resolution Imaging Spectroradiometer (MODIS): Land remote sensing for global change research. Ieee Transactions on Geoscience and Remote Sensing **36**:1228-1249.

Kampe, T. U. 2010. NEON: the first continental-scale ecological observatory with airborne remote sensing of vegetation canopy biochemistry and structure. Journal of Applied Remote Sensing **4**:043510.

Keller, M., D. S. Schimel, W. W. Hargrove, and F. M. Hoffman. 2008. A continental strategy for the National Ecological Observatory Network. Frontiers in Ecology and the Environment **6**:282-284.

Knapp, A. K., and S. L. Collins. 2019. Reimagining NEON operations: We can do better. BioScience **69**:956-959.

Kukal, M. S., and S. Irmak. 2018. U.S. Agro-Climate in 20th Century: Growing Degree Days, First and Last Frost, Growing Season Length, and Impacts on Crop Yields. Sci Rep **8**:6977.

Lark, T. J., B. Larson, I. Schelly, S. Batish, and H. K. Gibbs. 2019. Accelerated conversion of native prairie to cropland in Minnesota. Environmental Conservation **46**:155-162.

Lark, T. J., J. M. Salmon, and H. K. Gibbs. 2015. Cropland expansion outpaces agricultural and biofuel policies in the United States. Environmental Research Letters **10**:044003.

Leopold, A. and Jones, S.E., 1947. A phenological record for Sauk and Dane Counties, Wisconsin, 1935-1945. Ecological Monographs, **17**:81-122.

Liang, L. 2019. A spatially explicit modeling analysis of adaptive variation in temperate tree phenology. Agricultural and Forest Meteorology **266-267**:73-86.

Liang, L., M. Schwartz, and X. Zhang. 2016. Mapping temperate vegetation climate adaptation variability using normalized land surface phenology. Climate **4**:24.

Liang, L., M. D. Schwartz, and S. Fei. 2011. Validating satellite phenology through intensive ground observation and landscape scaling in a mixed seasonal forest. Remote Sensing of Environment **115**:143-157.

Liu, L., X. Zhang, A. Donnelly, and X. Liu. 2016. Interannual variations in spring phenology and their response to climate change across the Tibetan Plateau from 1982 to 2013. International Journal Of Biometeorology **60**:1563-1575.

Lobell, D. B., and G. P. Asner. 2003. Climate and management contributions to recent trends in U.S. agricultural yields. Science **299**:1032-1032.

Los, S. 2013. Analysis of trends in fused AVHRR and MODIS NDVI data for 1982–2006: Indication for a CO2 fertilization effect in global vegetation. Global Biogeochemical Cycles **27**:318-330.

Loveland, T. R., J. W. Merchant, J. F. Brown, D. O. Ohlen, B. C. Reed, P. Olson, and J. Hutchinson. 1995. Seasonal land-cover regions of the United States. Annals of the Association of American Geographers **85**:339-355.

Mascioli, N. R., M. Previdi, A. M. Fiore, and M. Ting. 2017. Timing and seasonality of the United States 'warming hole'. Environmental Research Letters **12**:034008.

McCabe, G. J., T. R. Ault, B. I. Cook, J. L. Betancourt, and M. D. Schwartz. 2012. Influences of the El Niño Southern Oscillation and the Pacific Decadal Oscillation on the timing of the North American spring. International Journal of Climatology **32**:2301-2310.

Medhaug, I., M. B. Stolpe, E. M. Fischer, and R. Knutti. 2017. Reconciling controversies about the 'global warming hiatus'. Nature **545**:41-47.

Meigs, G. W., R. E. Kennedy, A. N. Gray, and M. J. Gregory. 2015. Spatiotemporal dynamics of recent mountain pine beetle and western spruce budworm outbreaks across the Pacific Northwest Region, USA. Forest Ecology and Management **339**:71-86.

Morisette, J. T., Richardson, A. D., Knapp, A. K., Fisher, J. I., Graham, E., Abatzoglou, J., Wilson, B. E., Breshears, D. D., Henebry, G. M., Hanes, J. M., and Liang, L. 2009. Tracking the rhythm of the seasons in the face of global change: Challenges and opportunities for phenological research in the 21st Century. Frontiers in Ecology and the Environment **5**:253-260.

Nguyen, L. H., D. R. Joshi, D. E. Clay, and G. M. Henebry. 2020. Characterizing land cover/land use from multiple years of Landsat and MODIS time series: A novel approach using land surface phenology modeling and random forest classifier. Remote Sensing of Environment **238**:111017.

Nolan, C., J. T. Overpeck, J. R. M. Allen, P. M. Anderson, J. L. Betancourt, H. A. Binney, S. Brewer, M. B. Bush, B. M. Chase, R. Cheddadi, M. Djamali, J. Dodson, M. E. Edwards, W. D. Gosling, S. Haberle, S. C. Hotchkiss, B. Huntley, S. J. Ivory, A. P. Kershaw, S.-H. Kim, C. Latorre, M. Leydet, A.-M. Lézine, K.-B. Liu, Y. Liu, A. V. Lozhkin, M. S. McGlone, R. A. Marchant, A. Momohara, P. I. Moreno, S. Müller, B. L. Otto-Bliesner, C. Shen, J. Stevenson, H. Takahara, P. E. Tarasov, J. Tipton, A. Vincens, C. Weng, Q. Xu, Z. Zheng, and S. T. Jackson. 2018. Past and future global transformation of terrestrial ecosystems under climate change. Science **361**:920-923.

Norman, S. P., W. W. Hargrove, and W. M. Christie. 2017. Spring and autumn phenological variability across environmental gradients of Great Smoky Mountains National Park, USA. Remote Sensing **9**:407.

Oswalt, S. N., W. B. Smith, P. D. Miles, and S. A. Pugh. 2019. Forest Resources of the United States, 2017: a technical document supporting the Forest Service 2020 RPA Assessment. Gen. Tech. Rep. WO-97. Washington, DC: US Department of Agriculture, Forest Service, Washington Office. **97**.

Partridge, T. F., J. M. Winter, E. C. Osterberg, D. W. Hyndman, A. D. Kendall, and F. J. Magilligan. 2018. Spatially distinct seasonal patterns and forcings of the U.S. warming hole. Geophysical Research Letters **45**:2055-2063.

Piao, S., Q. Liu, A. Chen, I. A. Janssens, Y. Fu, J. Dai, L. Liu, X. Lian, M. Shen, and X. Zhu. 2019. Plant phenology and global climate change: current progresses and challenges. Global Change Biology **25**:1922-1940.

Reed, B. C. 2006. Trend analysis of time-series phenology of North America derived from satellite data. GIScience & Remote Sensing **43**:24-38.

Rocha, A. V., and G. R. Shaver. 2009. Advantages of a two band EVI calculated from solar and photosynthetically active radiation fluxes. Agricultural and Forest Meteorology **149**:1560-1563.

Rogers, J. C. 2013. The 20th century cooling trend over the southeastern United States. Climate Dynamics **40**:341-352.

Sacks, W. J., and C. J. Kucharik. 2011. Crop management and phenology trends in the US Corn Belt: Impacts on yields, evapotranspiration and energy balance. Agricultural and Forest Meteorology **151**:882-894.

Schimel, D., W. Hargrove, F. Hoffman, and J. MacMahon. 2007. NEON: a hierarchically designed national ecological network. Frontiers in Ecology and the Environment **5**:59-59.

Thorpe, A. S., D. T. Barnett, S. C. Elmendorf, E. L. S. Hinckley, D. Hoekman, K. D. Jones, K. E. LeVan, C. L. Meier, L. F. Stanish, and K. M. Thibault. 2016. Introduction to the sampling designs of the National Ecological Observatory Network Terrestrial Observation System. Ecosphere **7**:e01627.

Tomaszewska, M. A., and G. M. Henebry. 2018. Changing snow seasonality in the highlands of Kyrgyzstan. Environmental Research Letters **13**:065006.

Tomaszewska, M. A., L. H. Nguyen, and G. M. Henebry. 2020. Land surface phenology in the highland pastures of montane Central Asia: Interactions with snow cover seasonality and terrain characteristics. Remote Sensing of Environment **240**:111675.

Tucker, C. J. 1979. Red and photographic infrared linear combinations for monitoring vegetation. Remote Sensing of Environment **8**:127-150.

Wang, S. L., P. Heisey, D. Schimmelpfennig, and V. E. Ball. 2015. Agricultural productivity growth in the United States: Measurement, trends, and drivers. Economic Research Service, Paper No. ERR-189.

Wang, X., J. Xiao, X. Li, G. Cheng, M. Ma, G. Zhu, M. Altaf Arain, T. Andrew Black, and R. S. Jassal. 2019. No trends in spring and autumn phenology during the global warming hiatus. Nature Communications **10**:2389.

Weltzin, J.F., Betancourt, J. L., Cook, B. I., Crimmins, T. M., Enquist, C. A. F., Gerst, M. D., Gross, J. E., Henebry, G.M., Hufft, R.A., Kenney, M. A., Kimball, J.S., Reed, B. C., and Running, S.W. 2020. Seasonality of biological and physical systems as indicators of climatic variation and change. Climatic Change, accepted 11OCT20.

White, M., K. de Beurs, K. Didan, D. Inouye, A. Richardson, O. Jensen, J. O' Keefe, G. Zhang, R. Nemani, W. van Leeuwen, J. F. Brown, A. De Wit, M. Schaepman, X. Lin, M. Dettinger, A. S. Bailey, J. Kimball, M. D. Schwartz, D. D. Baldocchi, J. T. Lee, and L. W. K. 2009. Intercomparison, interpretation, and assessment of spring phenology in North America estimated from remote sensing for 1982-2006. Global Change Biology **15**:2335-2359.

White, M. A., F. M. Hoffman, W. W. Hargrove, and R. R. Nemani. 2005a. Phenoregions for Monitoring Vegetation Responses to Climate Change.*in* O. R. N. L. D. A. A. Center, editor., Oak Ridge, Tennessee, USA.

White, M. A., F. Hoffman, W. W. Hargrove, and R. R. Nemani. 2005b. A global framework for monitoring phenological responses to climate change. Geophysical Research Letters **32**:L04705.

Wright, C. K., and M. C. Wimberly. 2013. Recent land use change in the Western Corn Belt threatens grasslands and wetlands. Proceedings of the National Academy of Sciences **110**:4134-4139.

Yue, X., N. Unger, X. Zhang, and C. Vogel. 2015. Probing the past 30-year phenology trend of US deciduous forests. J Biogeosciences **12**:4693.

Zhang, X. 2015. Reconstruction of a Complete Global Time Series of Daily Vegetation Index Trajectory from Long-term AVHRR Data. Remote Sensing of Environment **156**:457-475.

Zhang, X. 2018. Land Surface Phenology: climate data record and real-time monitoring. Pages 35-52 *in* S. Liang, editor. Comprehensive Remote Sensing. Elsevier, Oxford.

Zhang, X., M. A. Friedl, C. B. Schaaf, A. H. Strahler, J. C. F. Hodges, F. Gao, B. C. Reed, and A. Huete. 2003. Monitoring vegetation phenology using MODIS. Remote Sensing of Environment **84**:471-475.

Zhang, X., S. Jayavelu, L. Liu, M. A. Friedl, G. M. Henebry, Y. Liu, C. B. Schaaf, A. D. Richardson, and J. Gray. 2018. Evaluation of land surface phenology from VIIRS data using time series of PhenoCam imagery. Agricultural and Forest Meteorology **256**:137-149.

Zhang, X., L. Liu, and G. M. Henebry. 2019. Impacts of land cover and land use change on long-term trend of land surface phenology: a case study in agricultural ecosystems. Environmental Research Letters **14**:044020.

Zhang, X., B. Tan, and Y. Yu. 2014. Interannual variations and trends in global land surface phenology derived from enhanced vegetation index during 1982–2010. International Journal of Biometeorology **58**:547-564.

Zhang, X., D. Tarpley, and J. T. Sullivan. 2007. Diverse responses of vegetation phenology to a warming climate. Geophysical Research Letters **34**:L19405.

Zhu, Z., S. Piao, R. B. Myneni, M. Huang, Z. Zeng, J. G. Canadell, P. Ciais, S. Sitch, P. Friedlingstein, A. Arneth, C. Cao, L. Cheng, E. Kato, C. Koven, Y. Li, X. Lian, Y. Liu, R. Liu, J. Mao, Y. Pan, S. Peng, J. Peñuelas, B. Poulter, T. A. M. Pugh, B. D. Stocker, N. Viovy, X. Wang, Y. Wang, Z. Xiao, H. Yang, S. Zaehle, and N. Zeng. 2016. Greening of the Earth and its drivers. Nature Climate Change **6**:791.

Zuckerberg, B., C. Strong, J. M. LaMontagne, S. St. George, J. L. Betancourt, and W. D. Koenig. 2020. Climate Dipoles as Continental Drivers of Plant and Animal Populations. Trends in Ecology & Evolution **35**:440-453.

Tables

Table 1.

Summary statistics of significant ($p<0.05$) changes in *start of season (SOS)* by NEON domains. Areas are in km^2. Areal percentages (%) were calculated based on the total actual area of each domain (including pixels with invalid values). Medians ($\tilde{x}$), means (μ), standardized deviations (σ), and coefficients of variation (*CV in %*) of the magnitudes of phenological shift (in days/decade) are provided. The asymmetry ratio (AR) was calculated by dividing the areal percentage of earlier trend by the areal percentage of later trend. Areal percentages of predominant trends (AR< 0.5/later or AR>2.0/earlier) are highlighted in bold with their corresponding AR values italicized.

ID	Domain Name	Earlier SOS						Later SOS						AR
		Area	*%*	$\tilde{x}$	μ	σ	*CV*	*Area*	*%*	$\tilde{x}$	μ	σ	*CV*	
1	Northeast	2,850	0.7	-2	-3	2	-73	21,200	**5.0**	3	3	2	55	*0.13*
2	Mid Atlantic	2,975	0.8	-1	-2	3	-153	98,875	**28.2**	4	4	3	67	*0.03*
3	Southeast	8,275	2.1	-1	-3	4	-139	166,050	**41.3**	4	5	4	77	*0.05*
4	Atl. Neotropical	350	1.3	-15	-12	5	-43	3,750	**14.0**	10	10	5	50	*0.09*
5	Great Lakes	1,400	0.3	-1	-2	3	-138	78,850	**19.5**	4	5	4	74	*0.02*
6	Prairie Peninsula	9,350	1.4	-1	-2	2	-106	291,825	**45.0**	7	8	5	61	*0.03*
7	Appalachians[a]	6,875	2.2	-2	-2	2	-63	37,150	**12.1**	5	7	5	75	*0.19*
8	Ozarks Complex	4,025	0.6	-2	-3	3	-126	137,900	**20.2**	5	6	4	77	*0.03*
9	Northern Plains	8,075	0.9	-3	-3	3	-80	251,350	**29.0**	5	5	3	61	*0.03*
10	Central Plains	2,750	0.6	-2	-3	3	-100	222,650	**49.1**	9	9	5	51	*0.01*
11	Southern Plains	2,750	0.5	-1	-2	2	-124	258,125	**48.2**	6	7	4	57	*0.01*
12	Northern Rockies	27,250	8.3	-4	-4	3	-77	45,750	14.0	5	5	3	65	0.60
13	Southern Rockies[b]	31,525	4.9	-5	-6	4	-73	145,275	**22.6**	8	9	5	58	*0.22*
14	Desert Southwest	2,250	0.5	-4	-5	5	-88	54,300	**12.4**	12	12	5	41	*0.04*
15	Great Basin	101,900	12.1	-4	-4	3	-66	52,400	6.2	4	5	4	77	1.94
16	Pacific Northwest	51,475	**27.7**	-6	-7	5	-64	7,800	4.2	4	5	4	80	*6.60*
17	Pacific Southwest	15,775	6.6	-7	-7	5	-67	14,900	6.2	6	7	5	71	1.06
18	CONUS	279,850	3.6	-4	-5	4	-81	1,888,150	**24.3**	6	7	5	67	*0.15*

[a]Appalachians / Cumberland Plateau; [b]Southern Rockies / Colorado Plateau

Table 2.

Summary statistics of significant ($p<0.05$) changes in *end of season (EOS)* by NEON domains. Areas are in km^2. Areal percentages (%) were calculated based on the total actual area of each domain (including pixels with invalid values). Medians ($\tilde{x}$), means (μ), standardized deviations (σ), and coefficients of variation (*CV in %*) of the magnitudes of phenological shift (in days/decade) are provided. The asymmetry ratio (AR) was calculated by dividing the areal percentage of earlier trend by the areal percentage of later trend. Areal percentages of predominant trends (AR< 0.5/later or AR>2.0/earlier) are highlighted in bold with their corresponding AR values italicized.

ID	Domain Name	Earlier EOS						Later EOS						AR
		Area	*%*	$\tilde{x}$	μ	σ	*CV*	*Area*	*%*	$\tilde{x}$	μ	σ	*CV*	
1	Northeast	750	0.2	-1	-1	1	-123	60,875	**14.4**	2	3	2	82	*0.01*
2	Mid Atlantic	12,625	3.6	-4	-5	3	-72	62,625	**17.9**	4	4	3	65	*0.20*
3	Southeast	7,800	1.9	-5	-5	4	-75	52,550	**13.1**	5	6	4	66	*0.15*
4	Atl. Neotropical	825	**3.1**	-11	-12	5	-41	375	1.4	10	11	6	60	*2.20*
5	Great Lakes	30,775	7.6	-3	-3	2	-59	94,400	**23.4**	2	3	2	85	*0.33*
6	Prairie Peninsula	284,225	**43.8**	-5	-5	3	-53	32,175	5.0	3	4	3	70	*8.83*
7	Appalachians[a]	38,025	12.4	-6	-7	4	-54	21,225	6.9	3	3	2	62	1.79
8	Ozarks Complex	57,375	8.4	-7	-7	4	-55	123,025	**18.0**	4	4	3	61	*0.47*
9	Northern Plains	102,800	11.9	-5	-6	4	-69	111,075	12.8	5	6	4	65	0.93
10	Central Plains	74,000	**16.3**	-8	-9	5	-53	7,900	1.7	4	4	3	72	*9.37*
11	Southern Plains	11,275	2.1	-8	-9	5	-63	31,950	**6.0**	4	5	4	78	*0.35*
12	Northern Rockies	21,350	6.5	-4	-6	5	-91	64,650	**19.8**	4	4	3	70	*0.33*
13	Southern Rockies[b]	8,775	1.4	-1	-3	4	-154	220,525	**34.3**	4	5	3	67	*0.04*
14	Desert Southwest	4,775	1.1	-11	-11	6	-53	13,000	**3.0**	6	7	5	64	*0.37*
15	Great Basin	112,075	13.3	-10	-10	6	-59	141,200	16.8	5	5	4	71	0.79
16	Pacific Northwest	18,875	10.2	-4	-6	5	-87	32,425	17.5	5	6	4	63	0.58
17	Pacific Southwest	34,350	14.3	-10	-10	6	-58	24,300	10.1	6	7	5	73	1.41
18	CONUS	820,675	10.6	-5	-7	5	-70	1,094,275	14.1	4	5	3	74	0.75

[a]Appalachians / Cumberland Plateau; [b]Southern Rockies / Colorado Plateau

Table 3.

Summary statistics of significant ($p<0.05$) changes in *growing season length (GSL)* by NEON domains. Areas are in km^2. Areal percentages (%) were calculated based on the total actual area of each domain (including pixels with invalid values). Medians ($\tilde{x}$), means (μ), standardized deviations (σ), and coefficients of variation (*CV in %*) of the magnitudes of phenological shift (in days/decade) are provided. The asymmetry ratio (AR) was calculated by dividing the areal percentage of earlier trend by the areal percentage of later trend. Areal percentages of predominant trends (AR< 0.5/longer or AR>2.0/shorter) are highlighted in bold with their corresponding AR values italicized.

ID	Domain Name	Shorter GSL						Longer GSL						AR
		Area	*%*	$\tilde{x}$	μ	σ	*CV*	*Area*	*%*	$\tilde{x}$	μ	σ	*CV*	
1	Northeast	7,725	1.8	-3	-3	2	-54	20,050	**4.7**	4	6	6	108	*0.39*
2	Mid Atlantic	33,550	**9.6**	-7	-8	6	-74	6,775	1.9	5	7	7	105	*4.95*
3	Southeast	36,400	**9.1**	-10	-13	10	-79	18,150	4.5	6	7	7	94	*2.01*
4	Atl. Neotropical	2,625	**9.8**	-20	-21	11	-53	100	0.4	10	12	8	67	*26.25*
5	Great Lakes	65,325	**16.2**	-6	-8	6	-74	13,900	3.4	5	7	6	90	*4.70*
6	Prairie Peninsula	348,275	**53.7**	-11	-12	7	-61	20,300	3.1	3	4	4	99	*17.16*
7	Appalachians[a]	40,800	13.3	-10	-13	9	-69	23,275	7.6	4	4	2	48	1.75
8	Ozarks Complex	84,100	**12.3**	-15	-17	12	-71	32,400	4.7	4	5	5	90	*2.60*
9	Northern Plains	194,375	**22.4**	-10	-10	6	-61	35,225	4.1	8	9	6	66	*5.52*
10	Central Plains	280,625	**61.9**	-14	-16	8	-54	7,225	1.6	5	6	5	85	*38.84*
11	Southern Plains	96,750	**18.0**	-14	-16	10	-62	9,875	1.8	5	9	9	106	*9.80*
12	Northern Rockies	29,175	8.9	-7	-8	7	-78	44,250	13.5	6	7	5	75	0.66
13	Southern Rockies[b]	108,775	16.9	-14	-15	9	-61	87,625	13.6	7	8	6	70	1.24
14	Desert Southwest	32,550	**7.4**	-20	-21	10	-49	3,000	0.7	8	12	10	87	*10.85*
15	Great Basin	200,150	**23.7**	-17	-18	11	-59	74,250	8.8	6	7	6	78	*2.70*
16	Pacific Northwest	10,750	5.8	-9	-11	9	-83	63,500	**34.2**	9	11	8	71	*0.17*
17	Pacific Southwest	19,225	8.0	-20	-20	12	-63	19,900	8.3	10	11	8	70	0.97
18	CONUS	1,591,175	**20.5**	-12	-14	9	-67	479,800	6.2	6	8	6	83	*3.32*

[a]Appalachians / Cumberland Plateau; [b]Southern Rockies / Colorado Plateau

Table 4.

Summary of significant ($p<0.05$) changes in start of season (SOS), end of season (EOS), and growing season length (GSL) over the entire CONUS relative to IGBP land cover types. Areas are in km^2. Areal percentages (%) were calculated based on the total area of each type of significant change across CONUS (as opposed to the total area of each land cover class). Areal percentages of the top two land cover types that contributed to each type of significant change are highlighted with underscores. The asymmetry ratio (AR) was calculated by dividing the area of earlier/shorter trend by the area of later/longer trend for each land cover class. Areas of predominant trends (AR< 0.5/later/longer or AR>2.0/earlier/shorter) are highlighted in bold with their corresponding AR values italicized.

Land Cover	Earlier SOS		Later SOS		AR	Earlier EOS		Later EOS		AR	Shorter GSL		Longer GSL		AR
	Area	%	Area	%		Area	%	Area	%		Area	%	Area	%	
ENF*	**611,92**	22.0	15,683	0.8	*3.90*	17,019	2.1	**39,991**	3.7	*0.43*	9,584	0.6	**77,194**	16.2	*0.12*
EBF	2,991	1.1	**9,410**	0.5	*0.32*	668	0.1	**8,277**	0.8	*0.08*	1,307	0.1	**4,995**	1.1	*0.26*
DBF	8,684	3.1	**66,623**	3.5	*0.13*	4,792	0.6	**85,355**	7.8	*0.06*	17,309	1.1	**37,755**	7.9	*0.46*
MF	1,220	0.4	**39,468**	2.1	*0.03*	1,772	0.2	**30,988**	2.8	*0.06*	10,078	0.6	5,925	1.2	1.70
CS	174	0.1	**523**	0.0	*0.33*	**1,655**	0.2	755	0.1	*2.19*	**639**	0.04	290	0.1	*2.20*
OS	1,655	0.6	**58,984**	3.1	*0.03*	4,502	0.5	**25,906**	2.4	*0.17*	**44,667**	2.8	4,618	1.0	*9.67*
WS	33,950	12.2	**238,784**	12.6	*0.14*	31,424	3.8	**247,961**	22.7	*0.13*	74,173	4.7	81,173	17.1	0.91
SA	11,239	4.0	**104,871**	5.6	*0.11*	9,119	1.1	**87,794**	8.0	*0.10*	34,821	2.2	29,420	6.2	1.18
GR	126,014	45.2	**631,462**	33.4	*0.20*	191,416	23.3	**400,519**	36.7	*0.48*	**602,042**	37.9	161,125	33.9	*3.74*
PW	813	0.3	**3,630**	0.2	*0.22*	726	0.1	**2,614**	0.2	*0.28*	1,597	0.1	1,481	0.3	1.08
CR	26,806	9.6	**678,423**	35.9	*0.04*	**548,227**	66.8	85,994	7.9	*6.38*	**776,295**	48.9	51,317	10.8	*15.13*
UBL	1,394	0.5	**26,051**	1.4	*0.05*	1,830	0.2	**56,284**	5.2	*0.03*	1,743	0.1	**13,679**	2.9	*0.13*
CNM	145	0.1	**4,211**	0.2	*0.03*	6,331	0.8	4,240	0.4	1.49	**7,115**	0.4	1,394	0.3	*5.10*

* Collection 6 MODIS land cover, MCD12C1 International Geosphere-Biosphere Programme (IGBP) classes: Evergreen Needleleaf Forests, ENF; Evergreen Broadleaf Forests, EBF; Deciduous Broadleaf Forests, DBF; Mixed Forests, MF; Closed Shrublands, CS; Open Shrublands, OS; Woody Savannas, WS; Savannas, SA; Grasslands, GR; Permanent Wetlands, PW; Croplands, CR; Urban and Built-up Lands, UBL; Cropland/Natural Vegetation Mosaics, CNM. (Water Bodies, WB; Deciduous Needleleaf Forests, DNF; Permanent Snow and Ice, PSI; and Barren, BA are omitted due to lack of vegetation changes.)

Figures

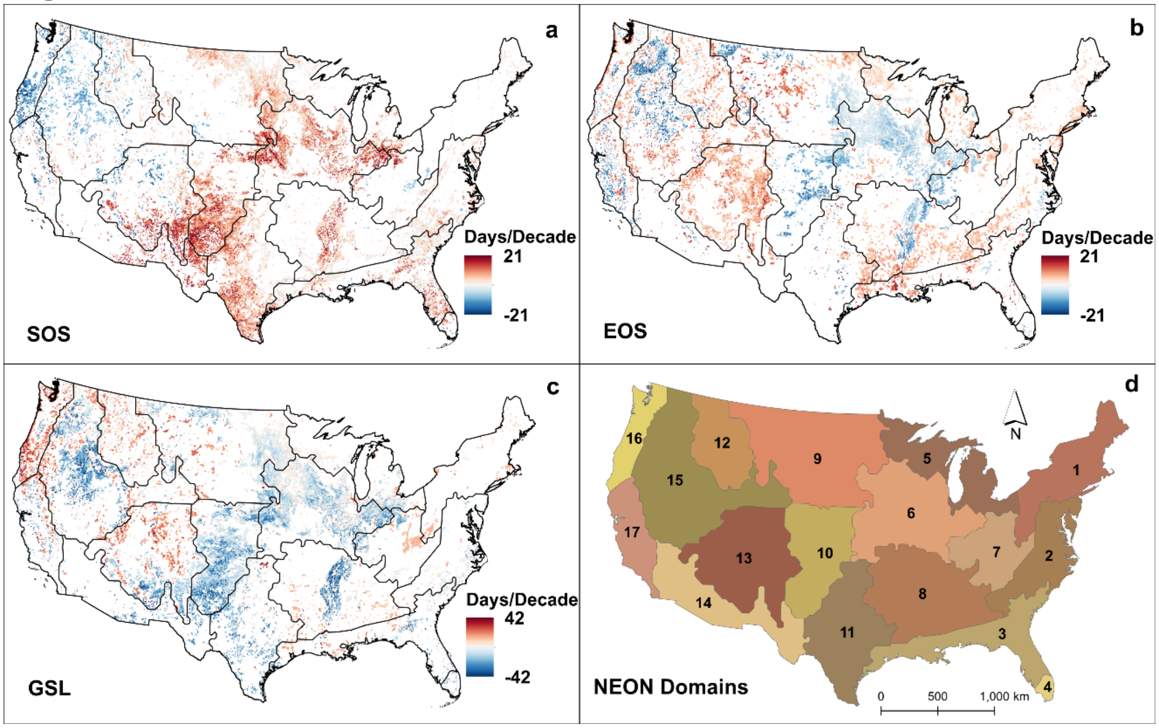

Figure 1.

Significant ($p < 0.05$) Theil-Sen median slopes of start of season (SOS), end of season (EOS), and growing season length (GSL) over the conterminous United States (a, b, c), 1982-2016. The trend maps are overlaid with boundaries of the NEON domains (d).

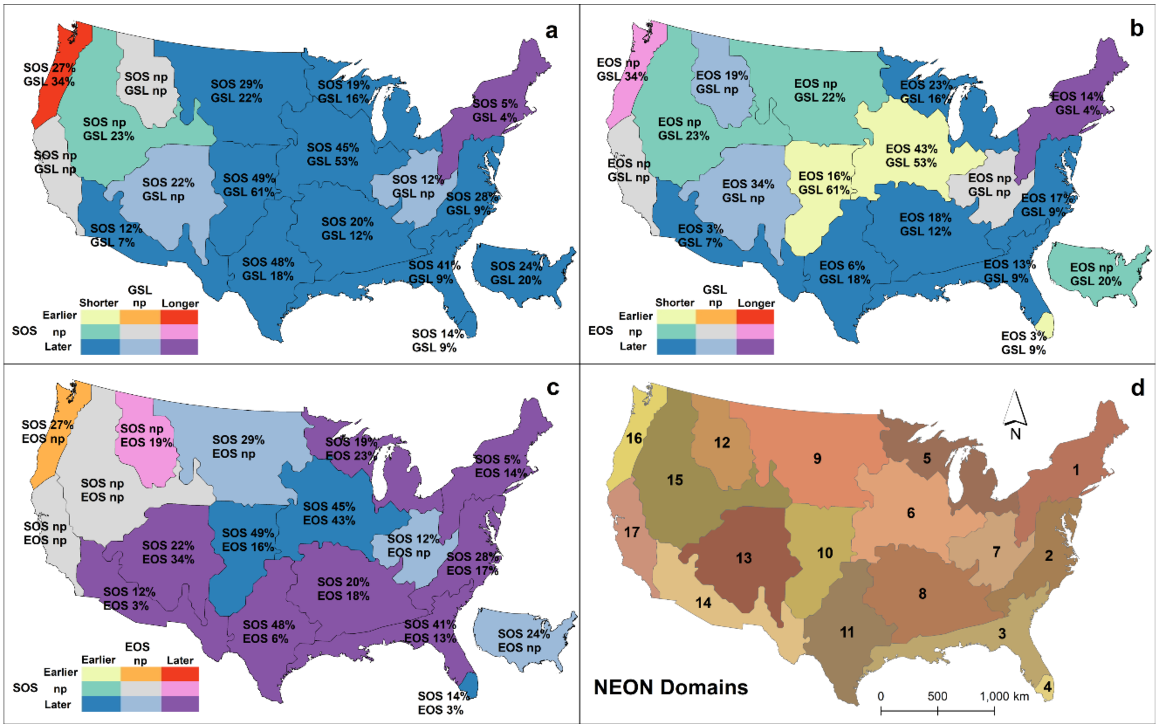

Figure 2.

Bivariate charts showing directions and percentage areas (rounded to integers) of predominant trends (1982-2016) in start of season (SOS), end of season (EOS), and growing season length (GSL) in respective NEON domains and across the conterminous United States.

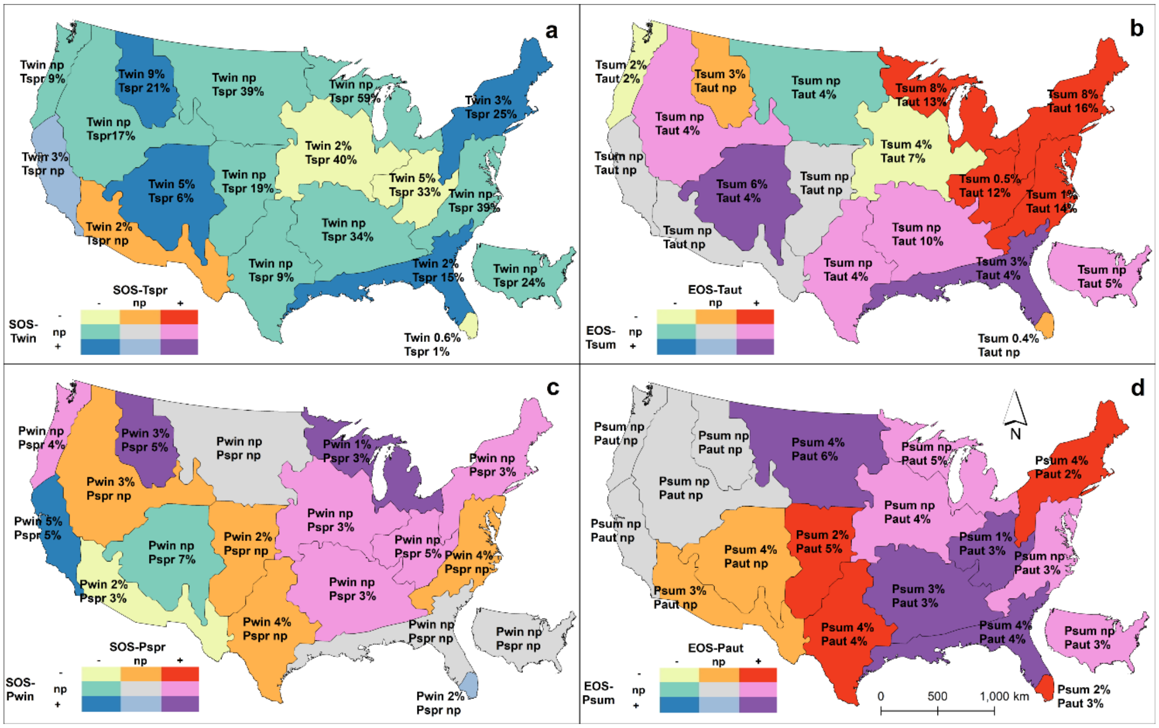

Figure 3.

Bivariate charts showing directions and percentage areas (rounded to integers except for values <1) of predominant partial correlations of start of season (SOS) respectively with winter temperature (Twin), spring temperature (Tspr), winter precipitation (Pwin), spring precipitation (Pspr), and of end of season (EOS) respectively with summer temperature (Tsum), autumn temperature (Taut), summer precipitation (Psum), and autumn precipitation (Paut) in respective NEON domains and across the conterminous United States.

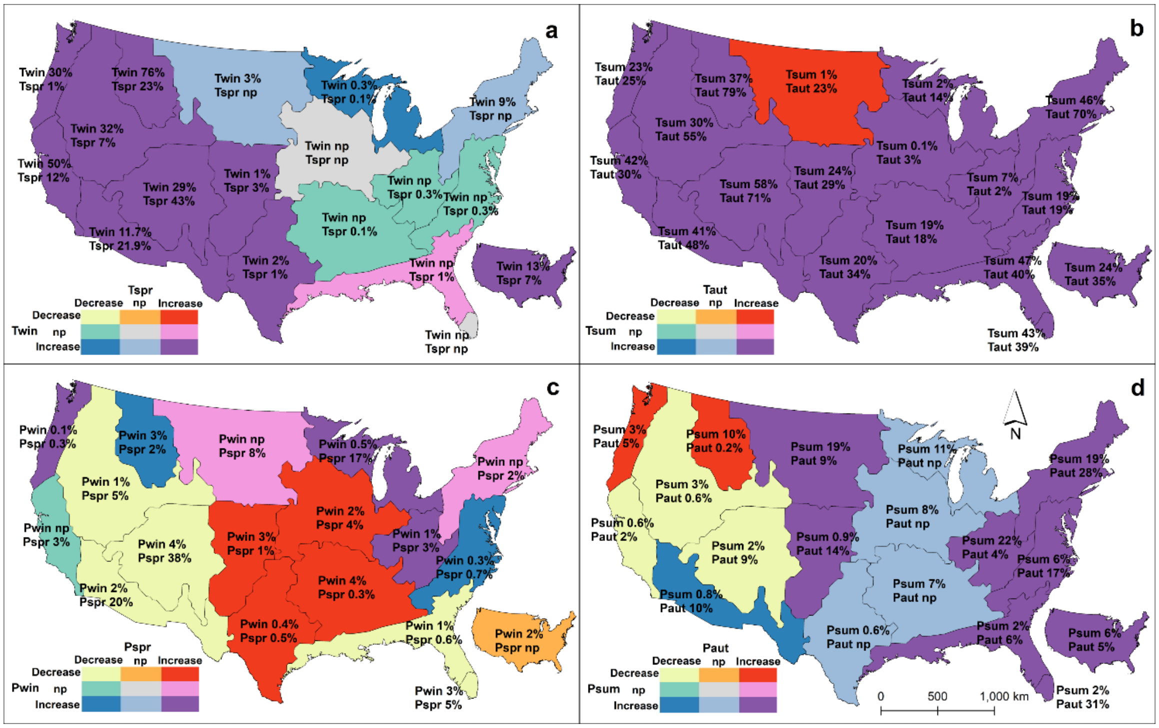

Figure 4.

Bivariate charts showing directions and percentage areas (rounded to integers except for values <1) of predominant trends (1982-2016) in winter temperature (Twin), spring temperature (Tspr), summer temperature (Tsum), autumn temperature (Taut), winter precipitation (Pwin), spring precipitation (Pspr), summer precipitation (Psum), and autumn precipitation (Paut) in respective NEON domains and across the conterminous United States.

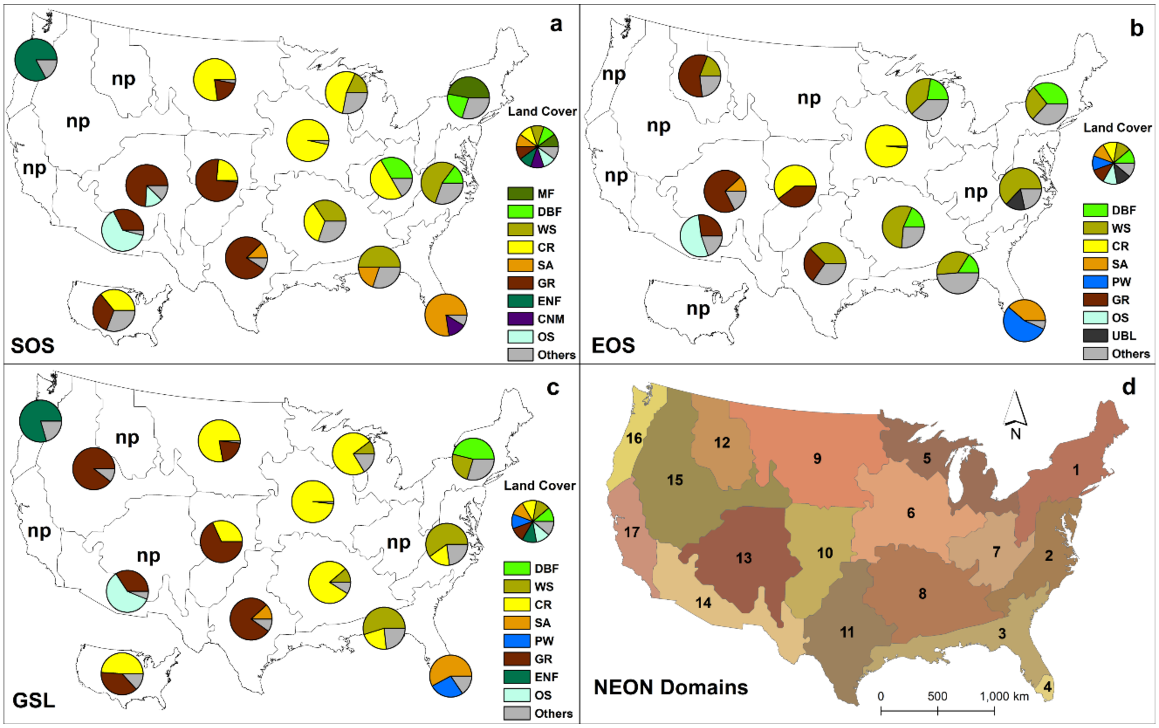

Figure 5.

Pie charts showing percentage areas of land cover contribution to the predominant trends (1982-2016) in start of season (SOS), end of season (EOS), and growing season length (GSL) in respective NEON domains and across the conterminous United States (*cf.* Tables S17-S19). Land cover types are according to collection 6 MODIS land cover, MCD12C1 International Geosphere-Biosphere Programme (IGBP) classes: Evergreen Needleleaf Forests, ENF; Evergreen Broadleaf Forests, EBF; Deciduous Broadleaf Forests, DBF; Mixed Forests, MF; Closed Shrublands, CS; Open Shrublands, OS; Woody Savannas, WS; Savannas, SA; Grasslands, GR; Permanent Wetlands, PW; Croplands, CR; Urban and Built-up Lands, UBL; Cropland/Natural Vegetation Mosaics, CNM. Only the classes ranked as the top two and with >10% area contribution are specified. Other classes with <10% area contributions are represented in the Others class.

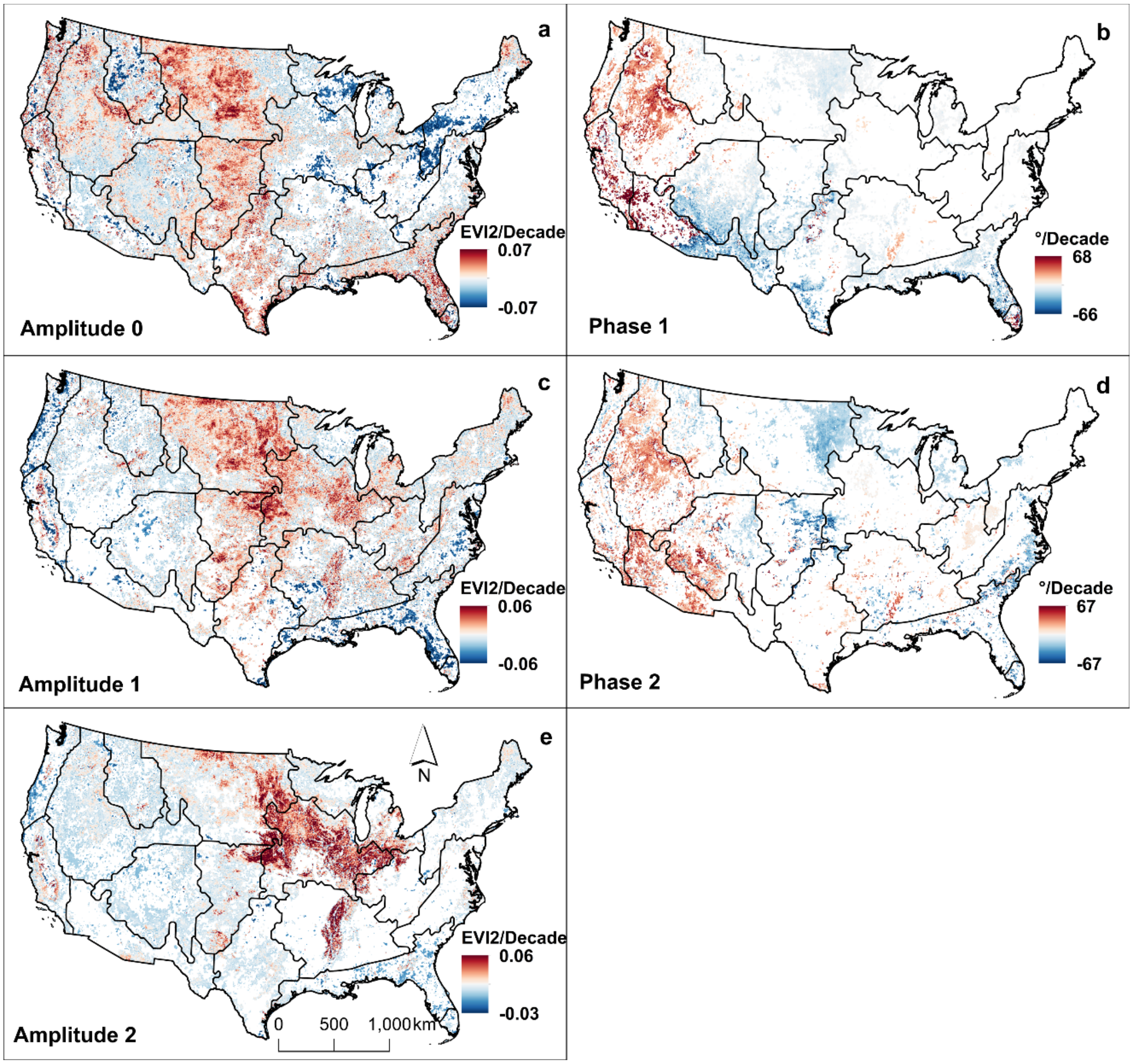

Figure 6.

Significant ($p<0.05$) Theil-Sen median slopes of the harmonic regression parameters (a-e) from 1982 to 2016. NEON domain boundaries are overlaid on each map. Amplitude 0 is the annual mean EVI2 value; Amplitude 1 is the amplitude of the annual cycle; Amplitude 2 is the amplitude of a semiannual cycle; Phase 1 is the location (in phase angle) of the beginning of the series on the annual cycle; and Phase 2 is the location of the beginning of series on a semiannual cycle. Amplitude changes indicate changes in greenness, while phase angle changes reflect seasonal changes (phenological changes), such as earlier shift of growing season (positive change) and later shift of growing season (negative change).

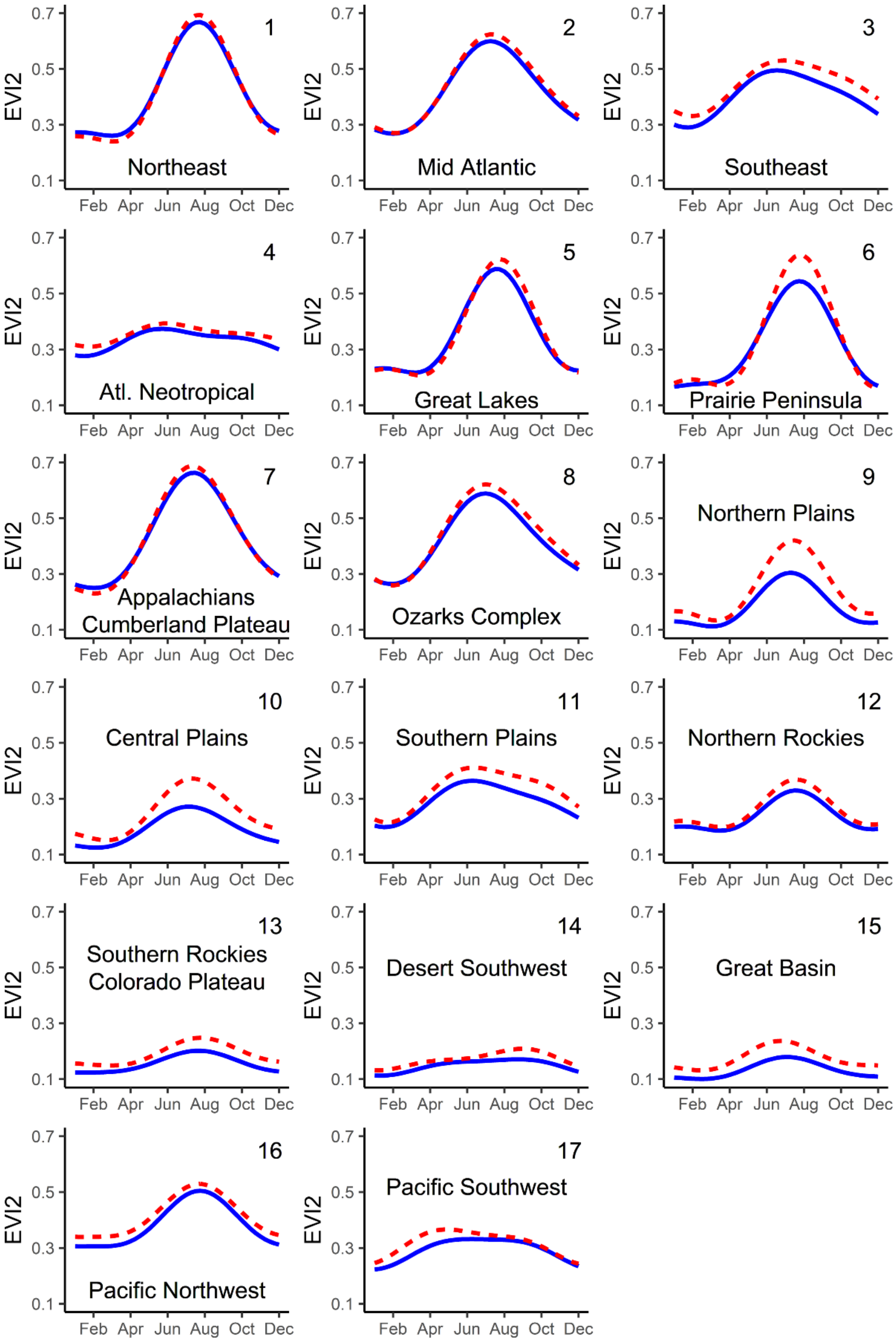

Figure 7.

Harmonic-regression-reconstructed annual EVI2 curves at the beginning (blue, solid line) and the end (red, dash line) of the study period (1982-2016) for respective NEON domains.